NAVAL POSTGRADUATE SCHOOL
Monterey, California

THESIS

Prototyping of Two-Beam Laser Interferometer
for Measurement of Optical Turbulence
Along Extended Paths

by

Carl Scott Barbour

December, 1992

Thesis Advisor: D.S. Davis
Second Reader: D.L. Walters

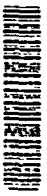

Approved for public release; distribution is unlimited

Unclassified

Security Classification of this page

REPORT DOCUMENTATION PAGE

1a Report Security Classification: Unclassified	1b Restrictive Markings
2a Security Classification Authority	3 Distribution Availability of Report: Approved for public release, distribution is unlimited
2b Declassification/Downgrading Schedule	
4 Performing Organization Report Number(s)	5 Monitoring Organization Report Number(s)
6a Name of Performing Organization: Naval Postgraduate School; 6b Office Symbol (If Applicable): PH/Dv	7a Name of Monitoring Organization: Naval Postgraduate School
6c Address (city, state, and ZIP code): Monterey, CA 93943-5000	7b Address (city, state, and ZIP code): Monterey, CA 93943-5000
8a Name of Funding/Sponsoring Organization: NPS; 8b Office Symbol (If Applicable)	9 Procurement Instrument Identification Number
8c Address (city, state, and ZIP code)	10 Source of Funding Numbers: Program Element Number; Project No; Task No; Work Unit Access or No

11 Title (Include Security Classification): PROTOTYPING OF TWO-BEAM LASER INTERFEROMETER FOR MEASUREMENT OF OPTICAL TURBULENCE ALONG EXTENDED PATHS

12 Personal Author(s): Carl Scott Barbour

13a Type of Report	13b Time Covered	14 Date of Report (year, month,day)	15 Page Count
Master's Thesis	From To	December 1992	46

16 Supplementary Notation: The views expressed in this thesis are those of the author and do not reflect the official policy or position of the Department of Defense or the U.S. Government.

17 Cosati Codes			18 Subject Terms (continue on reverse if necessary and identify by block number)
Field	Group	Subgroup	two-beam laser interferometer, optical turbulence. adaptive optics. phase comparator

19 Abstract (continue on reverse if necessary and identify by block number)

This thesis demonstrates a proof-of-concept experimental validation of a prototype two-beam, division of wavefront laser interferometer that provides real-time measurement of the optical path difference, and subsequent phase distortion, caused by atmospheric turbulence along an extended horizontal path. Prototype's signal processing incorporates use of specialized phase comparator circuit developed by author's advisor, D.S Davis. Photographs and results cited of the prototype receiver's output offer proof of the validity of the basic design. Further research of this technology is expected to support future laser/adaptive optics long range weapon applications.

20 Distribution/Availability of Abstract	21 Abstract Security Classification
[X] unclassified/unlimited [ ] same as report [ ] DTIC users	Unclassified
22a Name of Responsible Individual: D.S. Davis	22b Telephone (Include Area code): (408) 646-2877 — 22c Office Symbol: PH/Dv

DD FORM 1473, 84 MAR — 83 APR edition may be used until exhausted — All other editions are obsolete

security classification of this page: Unclassified

Approved for public release, distribution is unlimited

Prototyping of a Two-beam Laser Interferometer for Measurement of Optical Turbulence Along Extended Paths

by

Carl Scott Barbour

Lieutenant Commander, United States Navy
B.S , United States Naval Academy, 1980

Submitted in partial fulfillment of the
requirements for the degree of

MASTER OF SCIENCE IN ENGINEERING SCIENCE

from the

NAVAL POSTGRADUATE SCHOOL

December, 1992

Author 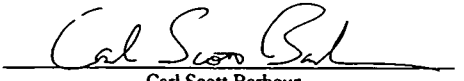
Carl Scott Barbour

Approved by 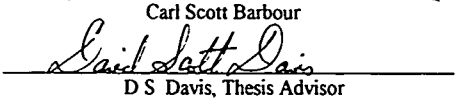
D S Davis, Thesis Advisor

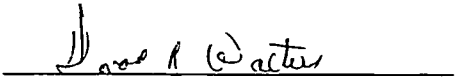
D L Walters, Second Reader

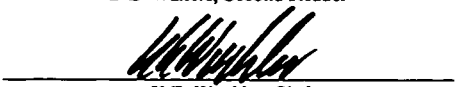
K E Woehler, Chairman,
Department of Physics

ABSTRACT

This thesis demonstrates a proof-of-concept experimental validation of a prototype two-beam, division of wavefront laser interferometer that provides a real-time measurement of the optical path difference, and subsequent phase distortion, caused by atmospheric turbulence along an extended horizontal path. Prototype's signal processing incorporates use of specialized phase comparator circuit developed by author's advisor, D.S. Davis. Photographs and results cited of the prototype receiver's output offer proof of the validity of the basic design. Further research of this technology is expected to support future laser/adaptive optics long range weapon applications.

TABLE OF CONTENTS

LIST OF FIGURES

I. INTRODUCTION

A. BACKGROUND

The development and proliferation of ballistic missile technology will have a preeminent impact on warfare in the foreseeable future. As demonstrated by Iraq in the recent 1991 Persian Gulf War, third world nations now possess the capacity to maintain, employ and even produce theater ballistic missiles. As documented by *Jane's Strategic Weapons Systems* [Ref. 1], nations ranging from Argentina to Iraq to North Korea are producing and exporting conventional theater ballistic missiles. Some of these missiles have the potential to carry chemical and nuclear payloads to ranges reaching 1000 km. Consequently, even in the post Cold War regimes of downsizing defense budgets, there exists in the United States the political consensus to develop the means to deter and to counter such threats. During the March 1991 Senate Armed Service Committee budget hearings, no less a spokesman than Senator Edward Kennedy (D-Mass.) strongly argued for increasing the portion of the Administration's Strategic Defense Initiative (SDI) budget allocated to theater ballistic missile defense (TBMD).

B. MOTIVATION

Given the political and military will to achieve an effective TBMD system, a wide range of proposals/programs are likely to be considered. Given the nature of the threat (high speed, high altitude, short reaction time) it is certain that one likely approach will seek to incorporate laser beam weapons and adaptive optic technology. Indeed, as reported by Graham P. Collins in *Physics Today* [Ref 2], such technology was considered by SDI for larger scale intercontinental ballistic Missile (ICBM) defense. The article reiterated one of the challenges of such laser-based systems, as follows:

Atmospheric turbulence promotes local variations in the medium's refractive index that distort wavefronts of light. Different portions of the wavefront travel different optical path lengths and consequently become out of phase with one another. This causes several undesirable effects, such as defocusing, beam wander and higher-order beam distortions

Without correction for atmospheric turbulence, the resulting loss of laser intensity/energy produced by such distortion would render any long range weapons application ineffective. The article further describes how adaptive optics can be used to correct this phase distortion, provided such systems are supplied with real-time measurements of the phase distortions encountered along the transmission path between weapon and target. Sophisticated real-time processing of the phase information is required because the adaptive mirror must be accurately deformed before the wavefront distortion changes by a significant fraction of the transmission wavelength. The time scale for such variations in distortion is typically of the order of a few milliseconds at optical wavelengths. [Ref 2: pp. 17-18]

Collins reported how this adaptive optical wavefront correction was achieved for transmission on vertical paths from the earth's surface through the atmosphere. In summary, there exists a relatively stable, uniform atomic sodium layer in the earth's atmosphere at altitudes of 90-100 km. A laser tuned to the 589 nm sodium line and aimed at this layer can create a bright "false star", or beacon of fluorescent sodium atoms, that will emit light back down through the atmosphere. As stated in the article, such a beacon lies above the major atmospheric contributions to wavefront distortion, which are significant at altitudes up to 20 km. Consequently, if you wish to image a high altitude or exo-atmospheric target, you radiate the portion of the sodium layer that lies on or near the same line of sight as the target. The resulting beacon provides light return which is distorted by the turbulence along the desired vertical transmission path. The distortion information provided by such light is used to adjust a deformable mirror to compensate for the distortion and correct the "image" of the target . [Ref 2: pp.18-19]

A laser weapon could use the same distortion information to correct its wavefronts, thereby enhancing the delivery of the lethal radiation to the target. However, any long range laser/adaptive optics weapon applications, including potential theater ballistic missile defense uses, are likely to involve skewed, non-vertical, atmospheric transmission paths. Such paths are devoid of natural sodium beacons and would be even more susceptible to turbulence/distortion as a result of greater variations in atmospheric conditions as a function of range. Consequently, measurements of the stratospheric phase distortion are needed in order to assess the performance of potential system designs.

C. THESIS GOAL

One of the first aspects in developing laser transmission applications over an extended low elevation paths is to obtain some baseline measurements on the magnitude of the time-dependent optical path difference created by turbulence. This thesis project has been devoted to the construction and testing of a prototype system designed by the author's advisor, D.S. Davis in collaboration with D.L. Walters. The project has been to develop a two-beam division of wavefront laser interferometer that provides a real-time measurement of the optical path difference, and subsequent phase distortion, caused by atmospheric turbulence along an extended horizontal path. The design, originally presented by Davis and Walters in a memorandum to Phillips Laboratory, combines a basic double-slit polarizing interferometer with a specialized receiver-processor [Ref. 3]. The latter is a modification of a proven signal processing system developed by Davis and used in a the tracking servo flown on NASA's Kuiper Airborne Observatory (KAO) [Ref. 4]. The complete system could be mounted in various platforms, both land-based and airborne, to provide optical path difference data over a variety of turbulent conditions, ranges, altitudes and geographic locations.

II. NATURE OF EXPERIMENT

A. GENERAL OVERVIEW

Atmospheric turbulence along an extended path will distort an initially planar optical wavefront due to local variations in the index of refraction, n. Hence n is a function, n(r), of location r. As developed by Robert K. Tyson in *Principles of Adaptive Optics* [Ref. 5], departure of wavefronts from ideal behavior can be mathematically modeled by a power series representation. The first order term of this series corresponds to the tilt of the wavefront over the transmission path. To measure this first order contribution to wave distortion, a two-beam division-of-wavefront interferometer can be used.

Consider two monochromatic, mutually coherent point sources that are radiating in phase as shown in Figure 1.

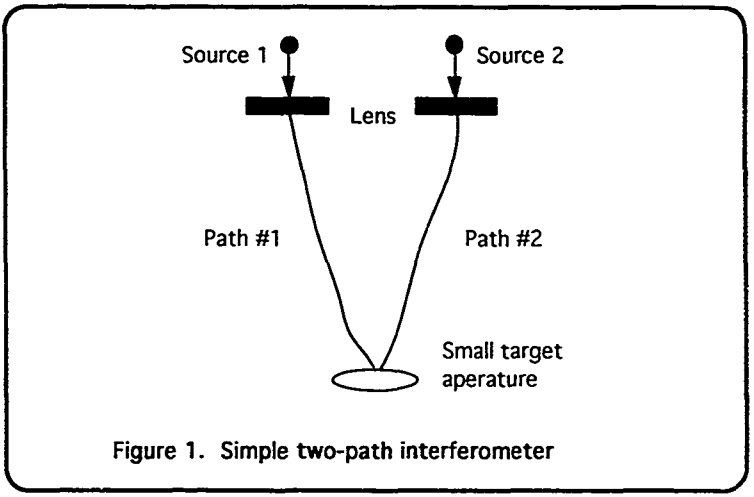

Figure 1. Simple two-path interferometer

A ray from source 1 reaches the target via path 1 and a similar ray from source 2 follows path 2. The integrated optical path length, δ_1, of the first ray is:

$$\delta_1 = \int^{\text{path 1}} n(r_1)\, dr\,, \tag{1}$$

while the path length for the second ray, δ_2, is:

$$\delta_2 = \int^{\text{path 2}} n(r_2)\, dr\,. \tag{2}$$

The relative coherence of the two rays reaching the target will be governed by the cosine of $2\pi\Delta$, where Δ is the optical path difference

$$\Delta = \delta_1 - \delta_2\,, \tag{3}$$

provided that Δ is much smaller than the intrinsic coherence lengths of the source This leads to the familiar Young's interference phenomenon at the target [Ref 6]. The proposed method of measuring Δ, the purpose of this thesis, will not rely on simple intensity interferometry. Rather, a more specialized approach will be employed to avoid phase ambiguity associated with any direct measurement of cosine $2\pi\Delta$.

B. SYSTEM DESIGN

1. Transmitter Design

As described by Davis [Ref 3], the basic optical transmitter configuration for the new approach is diagrammed in Figure 2.

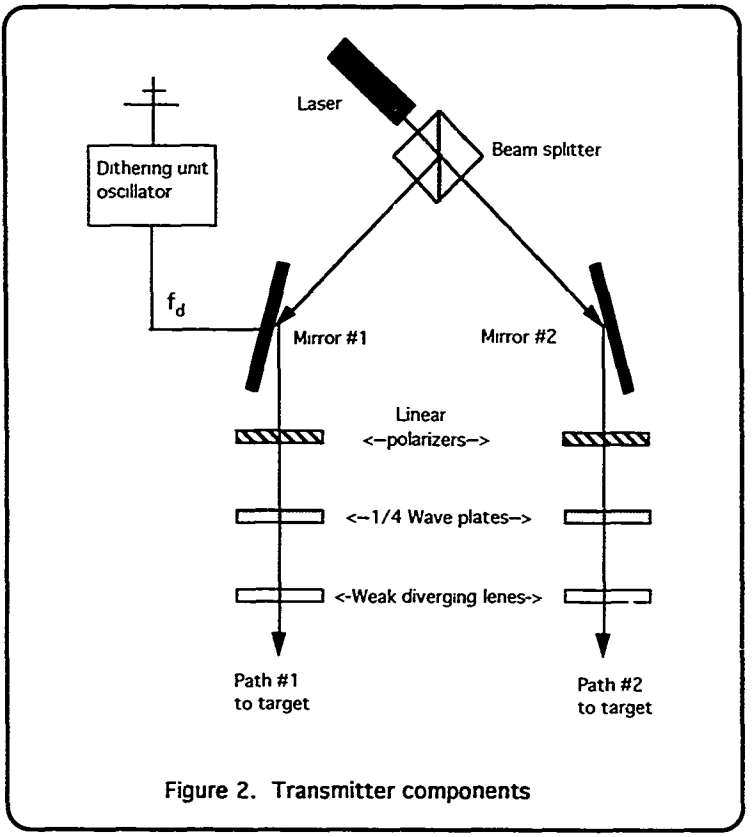

Figure 2. Transmitter components

A laser provides the coherent, unpolarized light source at a specified wavelength. (For the moment, assume the dithering unit and oscillator are not present.) The laser output passing through the beam splitter produces two beams of equal intensity with wavelength λ and angular frequency ω. The quarter-wave plates are arranged to produce right-circularly polarized radiation in one beam and left-circularly polarized in the other. E_o is the amplitude of the electric field in the outgoing beams. At the target/receiver, the electric fields of the two waves are:

$$\mathbf{E}_1 = E_0[\mathbf{i}\cos(k\delta_1-\omega t) + \mathbf{j}\sin(k\delta_1-\omega t)] \text{ and} \tag{4}$$

$$\mathbf{E}_2 = E_0[\mathbf{i}\cos(k\delta_2-\omega t) + \mathbf{j}\sin(k\delta_2-\omega t)] \tag{5}$$

where $k=2\pi/\lambda$. Both waves propagate in the +z direction, and it is assumed that source-to-target range is much larger than source-to-source separation so obliquity factors can be ignored. The interference of $\mathbf{E}_1$ and $\mathbf{E}_2$ at the target, $\mathbf{E}_t$, result in:

$$\mathbf{E}_t = E_o[\mathbf{i}(\cos(k\delta_1-\omega t)+\cos(k\delta_2-\omega t)) + \mathbf{j}(\sin(k\delta_1-\omega t)-\sin(k\delta_2-\omega t))] . \tag{6}$$

Now consider Θ, the instantaneous angle $\mathbf{E}_t$ makes with the +x axis:

$$\Theta = \tan^{-1}\left[\frac{\sin(k\delta_1-\omega t)-\sin(k\delta_2-\omega t)}{\cos(k\delta_1-\omega t)+\cos(k\delta_2-\omega t)}\right] . \tag{7}$$

Applying trigonometric identities,

$$\Theta = \frac{k}{2}(\delta_1-\delta_2) . \tag{8}$$

Hence Θ is independent of time, t. Consequently, the product of the interference of E_1 and E_2 is a linearly polarized wave with a polarization angle Θ that is a linear function of the optical path difference Δ:

$$\Theta = \frac{k\Delta}{2} . \tag{9}$$

Returning to the transmitter diagram in Figure 2, the function of the dithering oscillator and the dithering unit is to sinusiodally modulate the optical path difference Δ at a frequency f_d with amplitude ε. Consequently, equation (9) is modified such that the polarization angle Θ is now a function of both Δ and time, t:

$$\Theta = \frac{k}{2}[\Delta + \varepsilon \sin(\omega_d t)] \tag{10}$$

where $\omega_d = 2\pi f_d$.

2. Receiver Design

A complete block diagram of the receiver design is shown in Figure 3. For purposes of discussion, the receiver is divided into subassemblies of its optical and electronic signal processing components in the following sections.

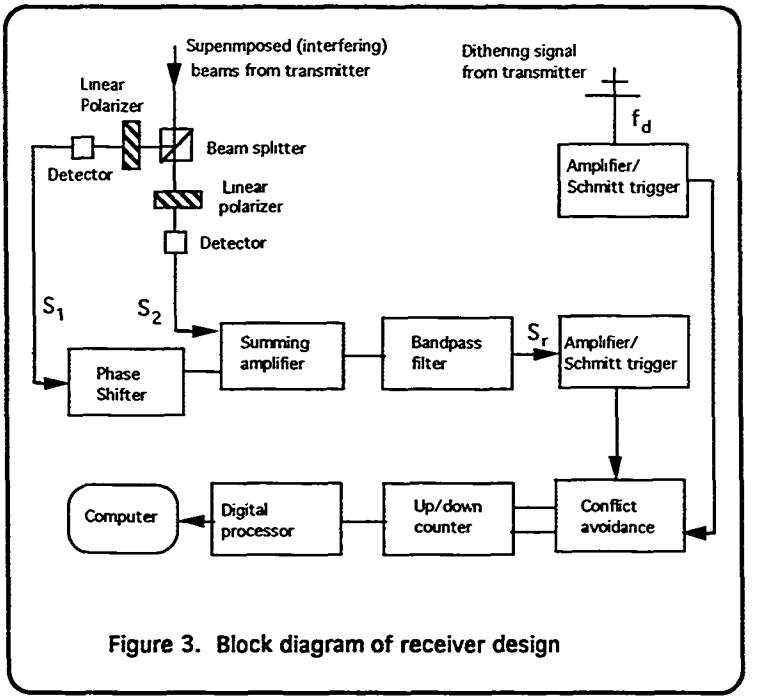

Figure 3. Block diagram of receiver design

a. Receiver Optics Design

As conceived by Davis, the two beams, one with its phase modulated at the dithering frequency f_d, transverse a horizontal atmospheric path. The optical path of each transmission will be affected by the turbulence each encounters enroute to a optical receiver/target configured as in Figure 4. [Ref. 3]

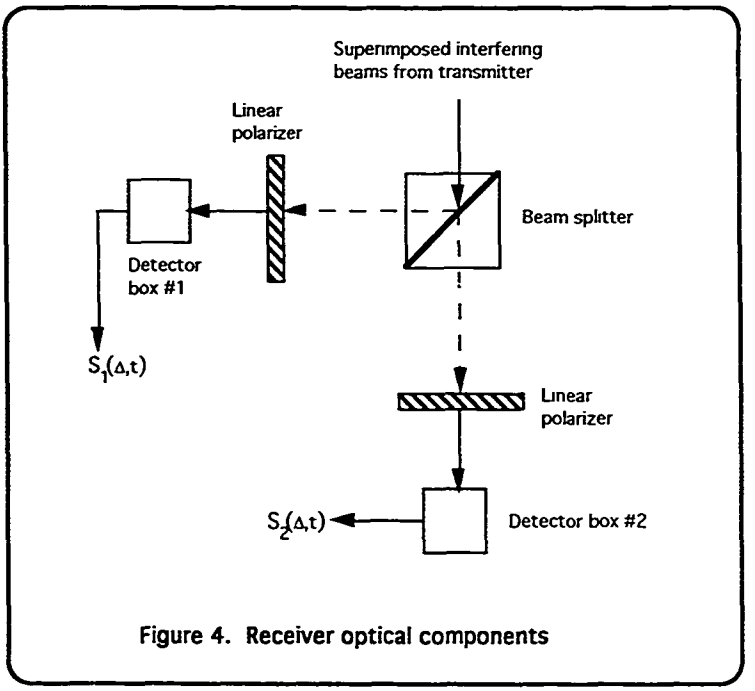

Figure 4. Receiver optical components

The linear polarizer before detector #1 has its axis oriented at 0 degrees; the polarizer before detector #2 is oriented at 45 degrees. Applying Malus's Law for transmitted intensifier [Ref 6: p. 259], the signals generated by each detector are:

$$S_1(\Delta,t) = S_0\cos^2[\frac{k}{2}(\Delta+\varepsilon\sin(\omega_d t))] \text{ and} \tag{11}$$

$$S_2(\Delta,t) = S_0\cos^2[\frac{k}{2}(\Delta+\varepsilon\sin(\omega_d t))+\frac{\pi}{4}] \tag{12}$$

with S_0 proportional to E_0^2.

b. Receiver Electronics Design

Both detector outputs, S_1 and S_2, now undergo initial signal processing as diagrammed in Figure 5.

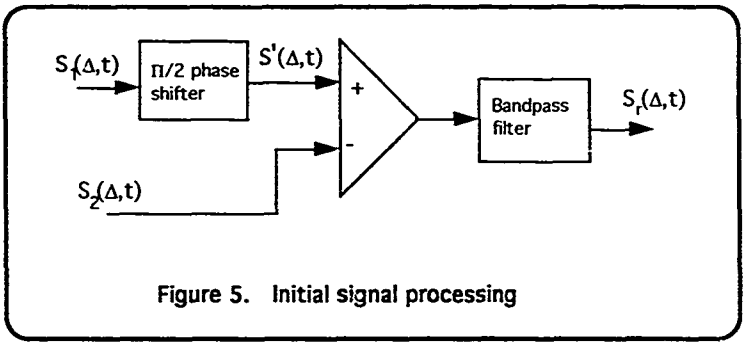

Figure 5. Initial signal processing

S_1 is passed through an electrical phase shifter to yield a $\pi/2$ phase shift at frequency, f_d. This produces a signal S_1' such that:

$$S_1'(\Delta,t) = S_0\cos^2[\frac{k}{2}(\Delta+\varepsilon\cos(\omega_d t))] . \tag{13}$$

Applying trigonometric identities for cosine squared yields:

$$S_1'(\Delta,t) = \frac{S_0}{2}[1+\cos(k(\Delta+\varepsilon\cos(\omega_d t))] \text{ and} \tag{14}$$

$$S_2(\Delta,t) = \frac{S_0}{2}[1-\sin(k(\Delta+\varepsilon\sin(\omega_d t))] . \tag{15}$$

As shown in Figure 5, these signals, when subtracted, yield:

$$S_r(\Delta,t) = \frac{S_0}{2}[\cos(k\Delta+k\varepsilon\cos(\omega_d t))+\sin(k\Delta+k\varepsilon\sin(\omega_d t))] . \tag{16}$$

The resulting signal $S_r(\Delta,t)$ is periodic with angular frequency, ω_d. The signal is then sent through a bandpass filter, $\omega_d/2 < \omega < 3\omega_d/2$, to remove the harmonic components. Applying the double angle trigonometric identities yields:

$$\begin{aligned} S_r(\Delta,t) = \frac{S_0}{2}[&\cos(k\Delta)\cos(k\varepsilon\cos(\omega_d t))-\sin(k\Delta)\sin(k\varepsilon\cos(\omega_d t)) + \\ &\sin(k\Delta)\cos(k\varepsilon\sin(\omega_d t))+\cos(k\Delta)\sin(k\varepsilon\sin(\omega_d t))] . \end{aligned} \tag{17}$$

Given a small dithering amplitude, ε, ($k\varepsilon << 1$) and small angle approximations for sine and cosine, there results:

$$S_r(\Delta,t) = \frac{S_0}{2}[\cos(k\Delta)-\sin(k\Delta)k\varepsilon\cos(\omega_d t)+\sin(k\Delta)+\cos(k\Delta)k\varepsilon\sin(\omega_d t)] . \tag{18}$$

The $\cos(k\Delta)$ and $\sin(k\Delta)$ terms are filtered out by the bandpass filter, leaving:

$$S_r(\Delta,t) = \frac{S_0}{2}k\varepsilon[\cos(k\Delta)\sin(\omega_d t)-\sin(k\Delta)\cos(\omega_d t)] . \tag{19}$$

Applying the double angle trigonometric identities, the remaining signal is at frequency, f_d.

$$S_r(\Delta,t) = \frac{S_0}{2} k\varepsilon \sin(\omega_d t - k\Delta) \tag{20}$$

which is a temporal signal of angular frequency ω_d, phase-modulated by the optical path difference. Δ.

From Figure 3, provision is made for transmitting the dithering signal f_d, via radio from the optical transmitter to the target/receiver. The receiver electronics will incorporate a radio receiver that will demodulate and reconstitute the dithering signal. In the receiver unit the phase of the dithering signal is compared to the phase of $S_r(\Delta,t)$ in a simple up-down counter, as shown in Figure 6.

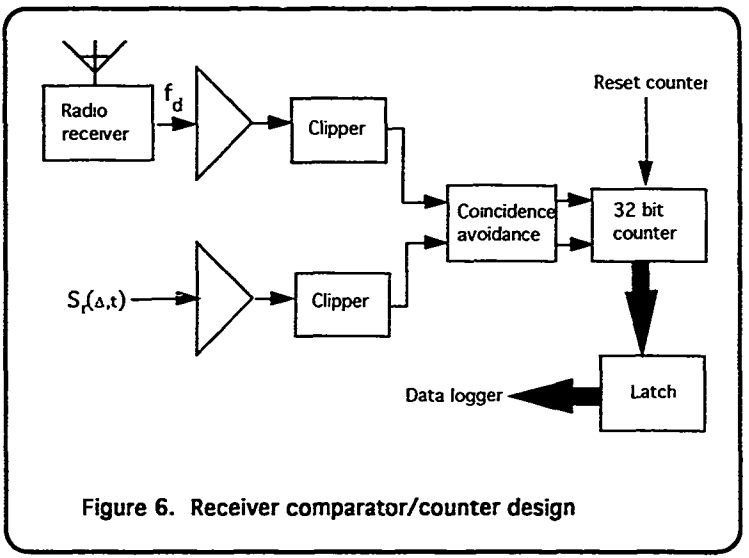

Figure 6. Receiver comparator/counter design

This phase comparator is a modification of an existing design that was developed by Davis and has been used successfully on the KAO Fourier transform spectrometer for many years. [Ref. 4]

When the system is operating, a change in the optical path difference Δ will alter the output count. An increase in the optical path difference Δ by wavelength λ results in a one-count increment; a decrease by wavelength λ results in a one count decrement. If dithering frequency f_d is chosen to be substantially higher than the highest fluctuation frequency of Δ (also known as the Greenwood frequency [Ref. 5: p. 36]), the oversampled data may be subsequently interpolated to reveal changes in Δ at the fractional values of λ. With dynamic range of $\pm 2^{31} \lambda$, the system can handle any conceivable variation. As an example, with λ= 632.8 nm, the available dynamic range for Δ is $\pm$ 1359 meters.

III. EXPERIMENTAL PROCEDURE

A. GENERAL APPROACH

The experiment as conducted during this thesis research represents a scaled-down laboratory prototype of the general design previously described in Chapter II. As a prototype system its function has been to test the basic theory, optical operation and signal processing electronics. The laboratory prototype system has a limited range of 200-300 ft. This limitation is primarily a function of two constraints, the transmission of the dithering signal and the power of the source laser. In the prototype, the dithering signal was transmitted by coaxial cable from the transmitter to the receiver instead of by radio. Furthermore a low power HeNe laser was used.

In addition, a digital to analog conversion circuit was added to the output of the receiver counter to facilitate monitoring of the receiver output signal/count on an oscilloscope. This removed the requirement for a computer/data-logger in the prototype. Electronic circuits were constructed using wire wrap techniques to allow for ease in assembly and modification as required.

B. PROTOTYPE ASSEMBLY

For discussion purposes, the description of the prototype construction is divided into transmitter and receiver assemblies.

1. Transmitter Assembly

As developed in Chapter II the transmitter's function is to generate superimposed interfering beams of left and right circularly polarized light that produce an optical interference pattern at the target/receiver. Figure 7 shows the optical configuration of the prototype transmitter. A photograph of the transmitter is shown in Figure 8.

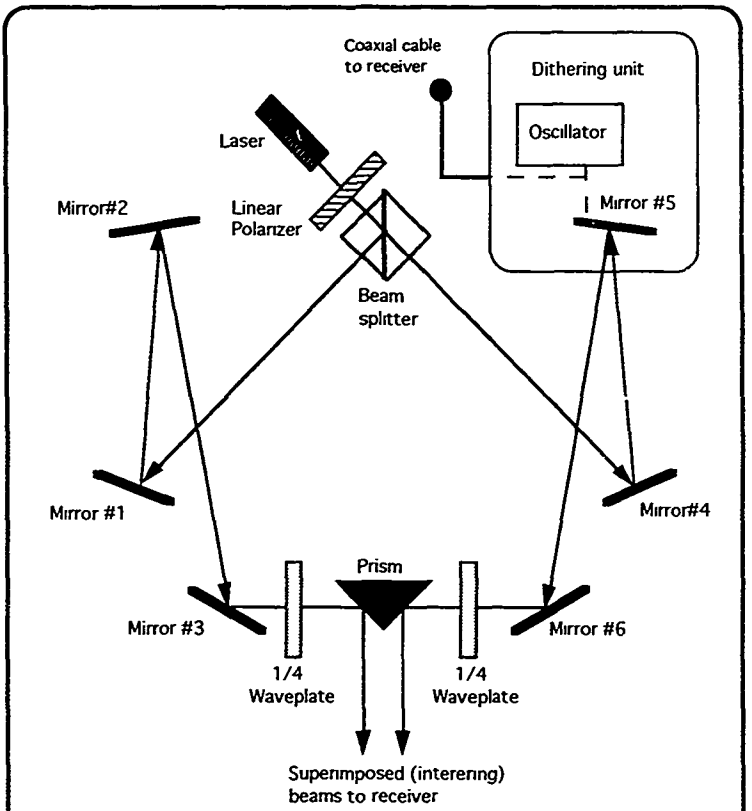

Figure 7. Schematic of prototype transmitter

Key aspects and components of the transmitter included:

- **Transmitter platform:** The transmitter was constructed on a 2 5' x 2.5' x 2 5/6" optical table, with internal damping and tapped surface mounting holes. This size table permitted easy portability of the system.

- **Optical arrangement:** Several mirror arrangements were tried using 2-3 mirrors in each beam path. The arrangement selected proved to be the most stable and easiest to align for the platform area available. All flat mirrors were mounted in 3-point adjustable holders (New Focus #9802). The beam splitter and prism were placed on adjustable prism holders (Melles Griot #07TTM003). To further facilitate beam path alignment, Mirror #3 (Figure 7) and the prism holders were mounted on adjustable micropositioners (Newport #4235).

- **Laser:** The laser was a 0.5mW, 632.8nm wavelength, helium-neon laser (Melles Griot #05 LLR 805). Detailed specifications are in Appendix (A). A linear polarizer was place directly in front of the laser to polarize the beam.

- **Optics:** All flat mirrors, with the exception of the dithering unit, were 25.4mm diameter mirrors (JML Direct #MPR15520/300). The beam splitter was a near-IR (650-900nm), 25.4mm cube type (Melles Griot #03BSD052). A coated, isosceles triangle prism was used as the output beam director.

- **Quarter-wave plates:** The quarter-wave plates were oriented to produce the prescribed right and left circularly polarized light in the respective beams per Equations (4) and (5). The plates were multiple order, 10mm diameter plates [Melles Griot #02WRQ021], mounted in standard polarizer holders [Melles Griot #007HPR001] with 10mm holder adapters [Melles Griot #07HPA001].

- **Dithering Unit:** The unit was a 1.55" x .60" rectangular flat mirror mounted on a piezoelectric translator (Physik Instrumente #249.10). An even smaller mirror should have been used in order to reduce the load placed on the translator, but one

was not available. The translator-mirror assembly was mounted on a piece of 25.4mm diameter aluminum stock which was placed in a optical holder The piezoelectric translator was connected to a signal generator electrically, which served as the dithering oscillator. The output of the dithering unit's oscillator was also connected to the receiver via coaxial cable.

Initial operational testing of the dithering unit as constructed revealed that its electro-mechanical resonant frequency was 13.2 kHz. However, after six days of sporadic operation, the resonant frequency dropped to 11.4 kHz. This frequency decrease coincided with a marked drop in lab ambient temperature, due to the onset of seasonal winter temperatures which apparently effected translator performance. Hence 11.4kHz was the dithering frequency, f_d, used during the ensuing experiment . A photograph the dithering unit is shown in Figure 9.

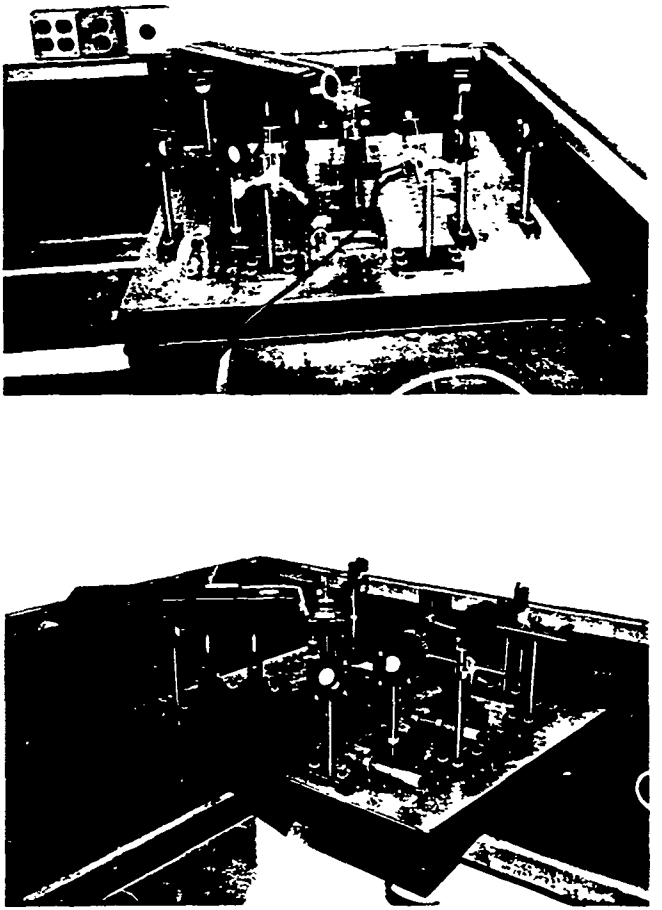

Figure 8. Photograph of prototype transmitter

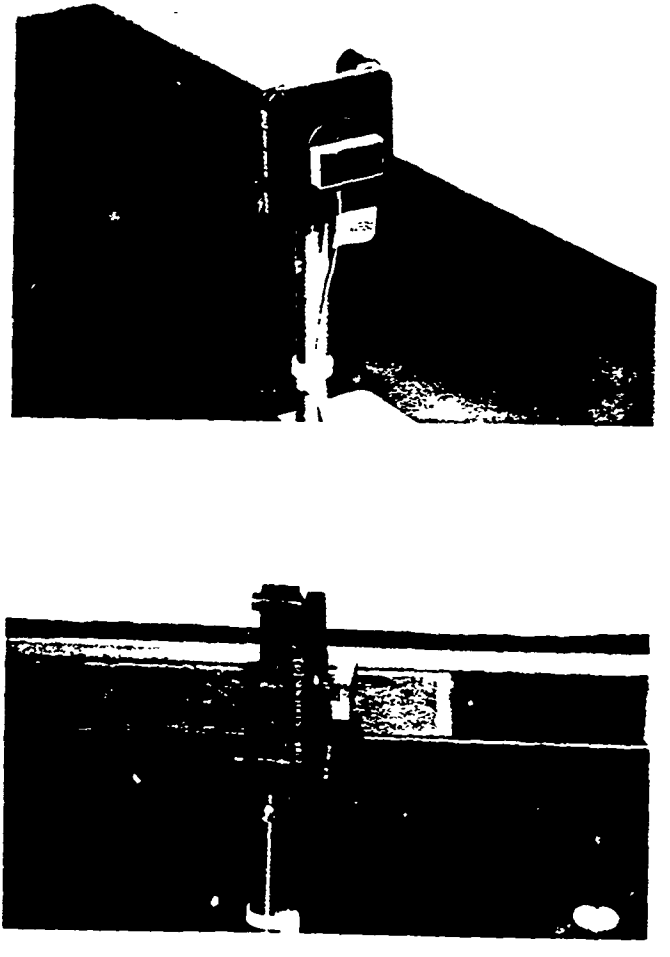

Figure 9. Photograph of dithering unit

2. Receiver Assembly

Figure 10 shows a complete block diagram of the entire prototype receiver assembly. As developed in Chapter II, the function of the receiver is to process optical detector signals from the transmitter's output beam. It must count the optical path difference/turbulence fringes encountered by the beam through its transmission path. For discussion purposes the receiver is divided into subassemblies for the receiver optics and the receiver electronics/signal processing.

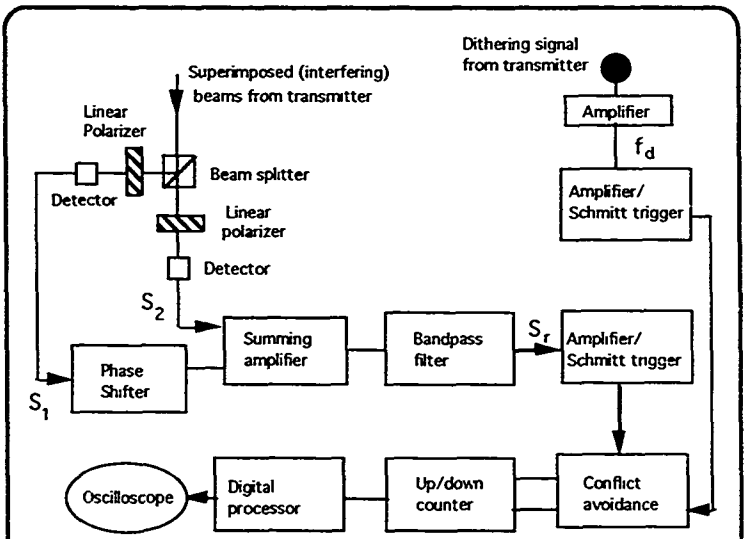

Figure 10. Block diagram of prototype receiver

a. Receiver Optics Assembly

Figure 11 is the optical configuration of the prototype receiver/target. A photograph of the receiver/target is shown in Figure 12 As developed in Chapter II, the receiver optics subassembly detects the transmitter's output beam and generates an electrical signal for later processing in the electronics subassembly.

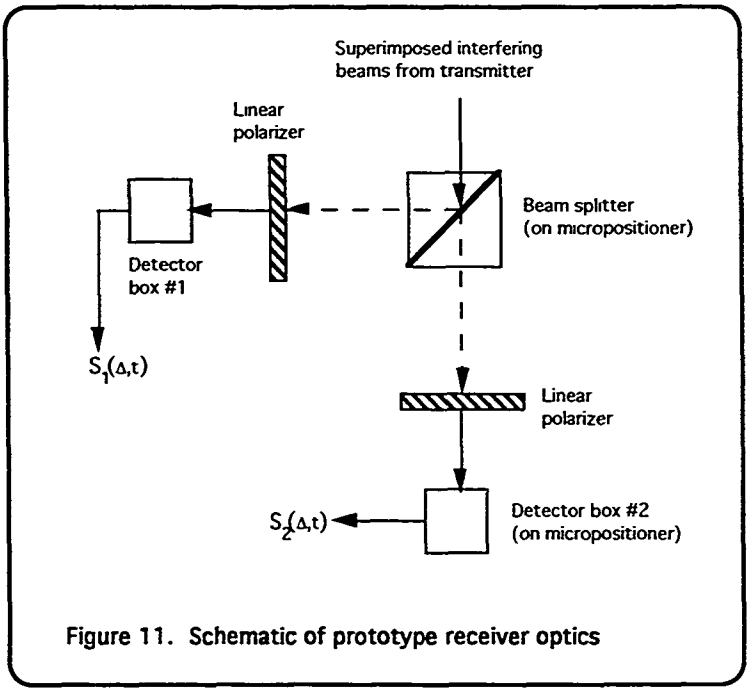

Figure 11. Schematic of prototype receiver optics

Key aspects and components of the receiver/target optics included:

- **Receiver platform:** The receiver was constructed on a 2.5' x 2.5' x 2 5/6" base which was identical to the one used for the transmitter. This size platform

allowed the ease of movement required in operating the system over various transmission paths.

- **Beam splitter:** The beam splitter was a near-IR (650-900nm), 25.4mm cube type (Melles Griot #03BSD052). The beam splitter sat on an adjustable micropositioner (Newport #4235) to facilitate beam alignment.

- **Linear polarizers:** Linear polarizers were placed in both beam paths between the beam splitter and the detectors. As presented in Figure 11, the polarizer in path #1 was set at 0 degrees, and the polarizer in path #2 was set at 45 degrees. This configuration allowed for the prescribed signal composition for later filtering per equations (11) and (12). The polarizers were 30.2mm diameter dichroic sheet polarizers, (Melles Griot #03FPG005), mounted in standard polarizer holders (Melles Griot #007HPR001) with 10mm holder adapters (Melles Griot #07HPA001).

- **Detectors:** The two detectors were blue-enhance silicon photodiodes (EG&G #UV-040BQ). These were selected for their low noise characteristics and wideband frequency response. Each photodiode was mounted in the wall of a shielded metal box using a circular rubber grommet insulator (see Figure 12). The box also enclosed the detector amplification circuitry and shielded against both external light and electrical noise. In addition, both detector boxes were also insulated from their respective supports. Detector #2 sat on an adjustable micropositioner (Newport #4235) to facilitate beam alignment.

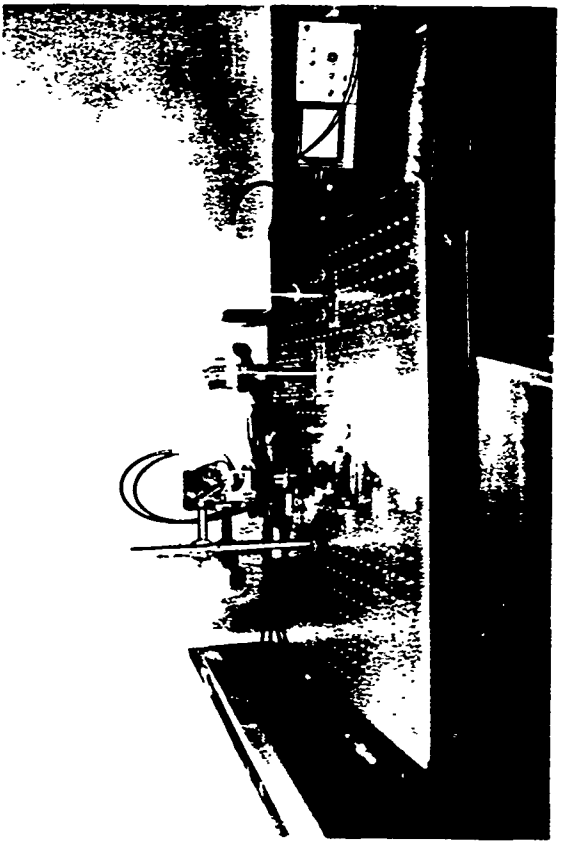

Figure 12. Photograph of receiver optics assembly

b. Receiver Electronics Assembly

(1) Detector Amplification Circuit. Each of the photodiodes was connected to a transimpedance amplifier [Ref. 7: p 235], like the one diagrammed in Figure 13. The entire circuit, including batteries, was enclosed within the detector boxes.

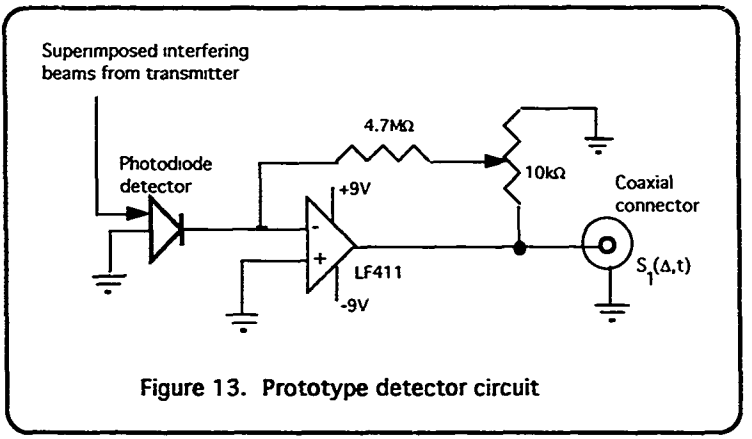

Figure 13. Prototype detector circuit

The National Semiconductor LF411 op amp was selected because of its high impedance and low noise. The 10 kΩ potentiometer allowed for output adjustment. The ±9V alkaline batteries were connected to a double pole toggle switch to turn the detector on/off. The gain adjustments were included so the two detector signals, S_1 and S_2 could be matched in amplitude.

(2) Initial Detector Signal Processing. Upon leaving the detector, signal S_1 undergoes the prescribed $\pi/2$ phase shift. This was accomplished by using a differentiator per equation (13) as shown in Figure 14 . The phase shifted signal is redesignated S_1'. Then both S_1' and S_2 are input to a summing amplifier, as diagrammed in Figure 14. The electronic behavior of the simple differientiator is described by

$$V_{out} = RC(\frac{dV_{in}}{dt}) , \tag{21}$$

where R=10kΩ and C=0.1μf. For sinusoidal input of the from V_{in}=Asin(ωt) the gain is further multiplied by the factor of ω (as a consequence of the differentiation). Consequently, S_2's adder was compensated to match the phase shifter's output. [Ref 7: p. 176]

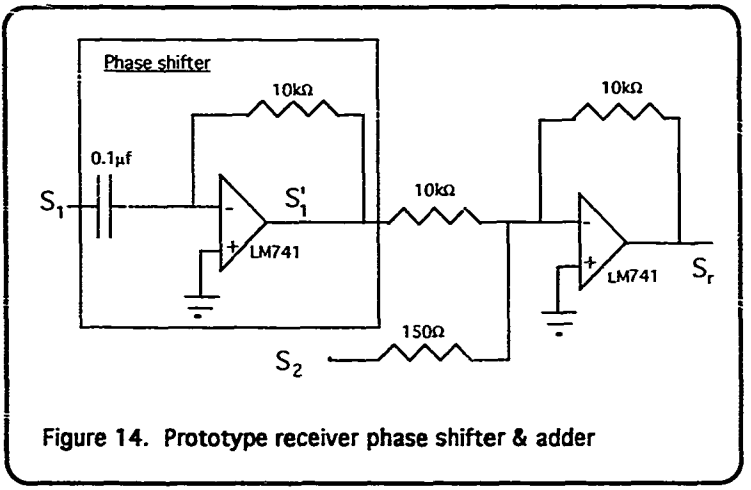

Figure 14. Prototype receiver phase shifter & adder

(3) Bandpass Filter Circuit. The combined signal that leaves the summing amplifier was bandpass-filtered with the characteristic response, $\omega_d/2 < \omega_d < 3\omega_d/2$ per equation (19). This was accomplished by the circuit in Figure 15. This circuit was selected for the relative ease with which the quality factor, Q, and the gain, G, could be varied and the ease in setting the center frequency, f_o. [Ref. 7]. The component values in Figure 15; C = .01 μf, R_F = 1.2 kΩ, R_1 = 47 kΩ, R_G = 2.2kΩ and R_Q = R = 10 kΩ, result in the following response characteristics:

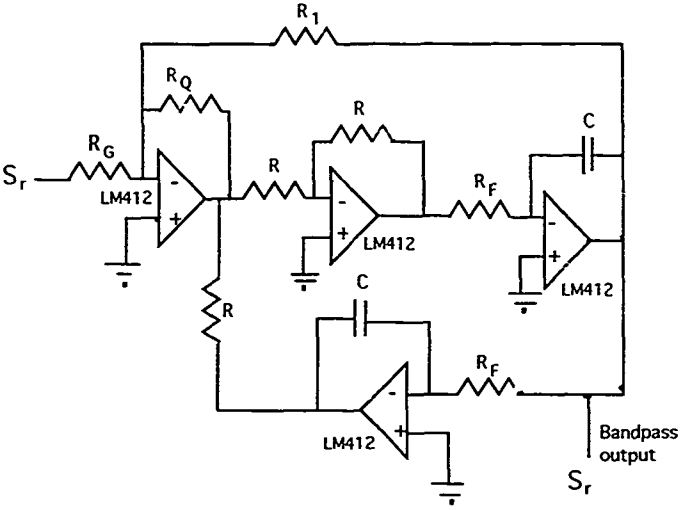

Figure 15. Prototype receiver bandpass filter

$$f_0 = \frac{1}{2\pi RC} = 13.263 \text{ kHz} \tag{22}$$

$$Q = \frac{R_1}{R_Q} = 4.7 \tag{23}$$

$$G = \frac{R_1}{R_G} = 21 \tag{24}$$

The National Semiconductor LM412 op amps were selected because their twin amp per 8-dip chip reduced circuit size and for their low internal impedance.

(4) Phase Comparator Circuit. At the very heart of the receiver system was the phase comparator circuitry. It is shown in detail in the schematic diagram of Figure 16. The version shown in the figure has a 16 bit dynamic range, but for simplicity the prototype used only an 8 bit dynamic range. The phase comparator really consisted of three parts: a pair of Schmitt trigger input conditioners, a conflict avoidance module, and an up-down binary counter with latched output lines. Each of these is described in more detail below.

The Schmitt trigger input conditioners appeared on both the dithering phase reference signal and the phase modulated signal lines. They were of conventional design [Ref 7: p. 231], employing LM311 comparator chips and $\pm$ 2V hysteresis thresholds. They had a twofold purpose: (1) to square up the analog input signals so that they conform to standard TTL-CMOS logic levels (0-5V), and (2) to provide high noise immunity ($\pm$ 2V) against noise pickup on the signal lines.

The conflict avoidance was the most complicated part of the phase comparator. It had a straightforward function. The cascaded up-down counters that actually track phase differences cannot respond to simultaneous count up and count down commands. The conflict avoidance module prevents such simultaneous counts by delaying the phase modulated signal progress. After a count up is completed, the delayed count down is executed. The two count pulse trains are always separated in time by a least 500ns, in order to accommodate propagation delays in the counters.

The up-down counter is very simple [Ref 7: p. 524]. Provision is made for setting the cascaded counter train to mid-count, corresponding to a "zero" phase difference between the two input signals. The counter outputs are latched in order to suppress ripple glitches that may occur during counter transitions.

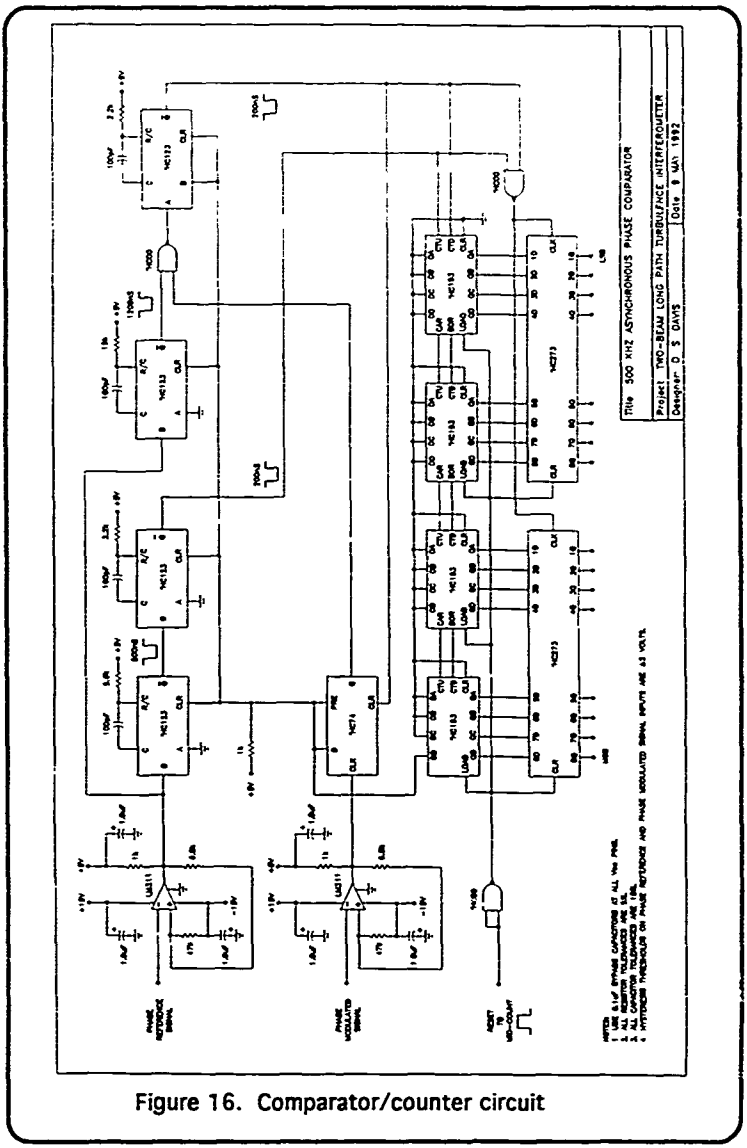

Figure 16. Comparator/counter circuit

(5) Digital-analog Conversion. A field-deployable version of the apparatus will have a dedicated computer to process the output from the phase comparator. Basically, this computer will perform a running mean on the stream of binary numbers from the phase comparator. This running mean constitutes an interpolated, low-pass filtered analog of the desired optical path difference Δ.

The prototype system developed during this thesis research did not have access to a dedicated computer. Hence, a direct way of displaying the output was developed, using a digital-to-analog converter (DAC) and low-pass filter, feeding an oscilloscope (see Figure 17). The cutoff frequency, f_c, for the filter is 3.38kHz.

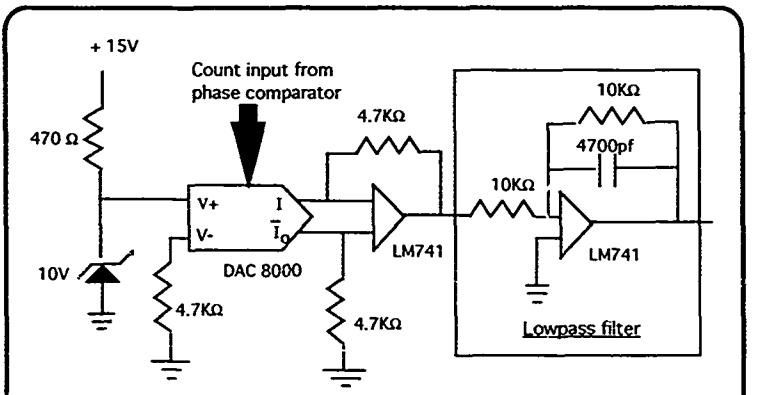

Figure 17. Prototype D/A converter & lowpass filter

C. PROTOYPE OPERATION/RESULTS

1. Component Testing and Operation

Upon completion of the prototype, individual components were operated and tested to design requirements. This process uncovered several areas requiring additional refinement that were not discovered during component construction. Some of these items have been cited in the previous sections, but summary of all the initial operational problems follows.

a. Transmitter Optical Alignment

Maintaining the correct transmitter optical alignment to produce the desired interference pattern at the receiver proved to be an ongoing maintenance problem. Any significant vibration of the optical platform would require rechecking and adjusting various optical components. Unfortunately such vibrations are prevalent in the laboratory environment in which this work was conducted.

b. Dithering Signal Amplification

The output of the dithering oscillator was restricted to a sinusoidal amplitude of less than 2-3 volts so as not to overdrive the piezoelectric translator. This same signal was insufficient to meet the $\pm$ 2V minimum voltage to drive the reference signal's Schmitt trigger at the receiver after traversing several feet of coaxial cable between the dithering oscillator and the receiver assembly. Consequently, a simple signal amplifier (LM741) was added prior to the the reference signal's Schmitt trigger. The amplifier provided a signal gain of 4.7 which proved sufficient to drive the triggers.

c. Detector Signal Loading

Upon initial operation, it was discovered that the S_2 detector signal from detector #2 was not reaching the receiver adder. Further investigation determined that the 4.7MΩ feedback resistance in the detector amplifications circuit loaded down the signal when compared to the 150 Ω input resistor at S_2's adder input. This problem was

corrected by placing a National Semiconductor LM 310 voltage follower/buffer between the detector amplification circuit and the summer.

d. Detector Signal Interference

The final hurdle in the prototype's operation concerned a 10 2kHz random signal of undetermined origin that showed up as unwanted noise on both detector signals. This noise signal was especially troublesome as the frequency was near the prototype's dithering frequency of 11.2kHz and it made matching the detector amplitudes difficult. While the source was never discovered, its impact was eliminated by further electrically isolating the detector boxes. The metal support posts for each detector were replaced with plastic posts. In addition, the detector boxes themselves were connected to the circuit ground through 100Ω resisitors. These changes successfully eliminated most of the interference. Observations of the two detectors' outputs on an oscilloscope showed that the peak-to-peak modulation produced by the optical fringes was at least 20 time higher than the noise on either detector channel.

2. Prototype Operation

With the aforementioned problems corrected the entire system underwent a complete operational test. This initial test was conducted in a laboratory with the transmitter and receiver optical platforms placed on a level lab bench. The optical transmission distance between the transmitter's prism and the receiver's beam splitter was 1.73 meters. The operation was conducted at night with the room dark to ensure the detector signals were the sole result of the transmitter's laser.

Figure 18 shows the Lissajous figure produced by feeding one detector output to the x-input of an oscilloscope, while the other detector is fed to the y-input. Recall equations (11) and (12) from Chapter II These equations, when combined with the trigonometric identities

$$\cos^2\Theta = \frac{1}{2}(1+\cos 2\Theta) \text{ and} \tag{25}$$

$$\cos(\Theta+\frac{\pi}{2}) = -\sin\Theta \ , \tag{26}$$

predict that ideal instrumental performance will yield a perfectly circular Lissajous figure in the presence of wavefront turbulence. A change of optical path difference Δ by one optical wavelength will result in a Lissajous phase change of 2π, corresponding to one complete rotation of the pattern on the oscilloscope screen. Figure 18 demonstrates that, while the prototype system is not perfect (i.e. the Lissajous figures are not perfectly circular), its basic properties are fundamentally correct.

To gauge the operation of the receiver signal processing and measure turbulence, an oscilloscope displayed the receiver's filtered digital-to-analog output. During operation artificial turbulence was introduced by waving a fan near the transmission path. This action produced one and two increments shifts in the receiver's digital-to-analog converter output that represented one and two wavelength path differences between the two superimposed beams from the transmitter. The receiver counter output was further exercised by inducing fringe shifts simulating turbulent effects by tapping on the lab bench supporting the apparatus. Such results confirmed the basic design operation of the prototype. However sustained system operation proved difficult. Any slight change in detector signals, due either to changes in optical alignment and/or interference, necessitated extensive alterations to the signal processing components to insure that detector signal amplitudes remained matched and of sufficient strength to meet the 2V input requirements of the Schmitt trigger. The system's fragility and lack of robustness was difficult to address given the resource/equipment limitations of the prototype. Further, more involved, development and

testing with higher precision, more stable components is required Recommendations for future operational tests will be made in the following sections.

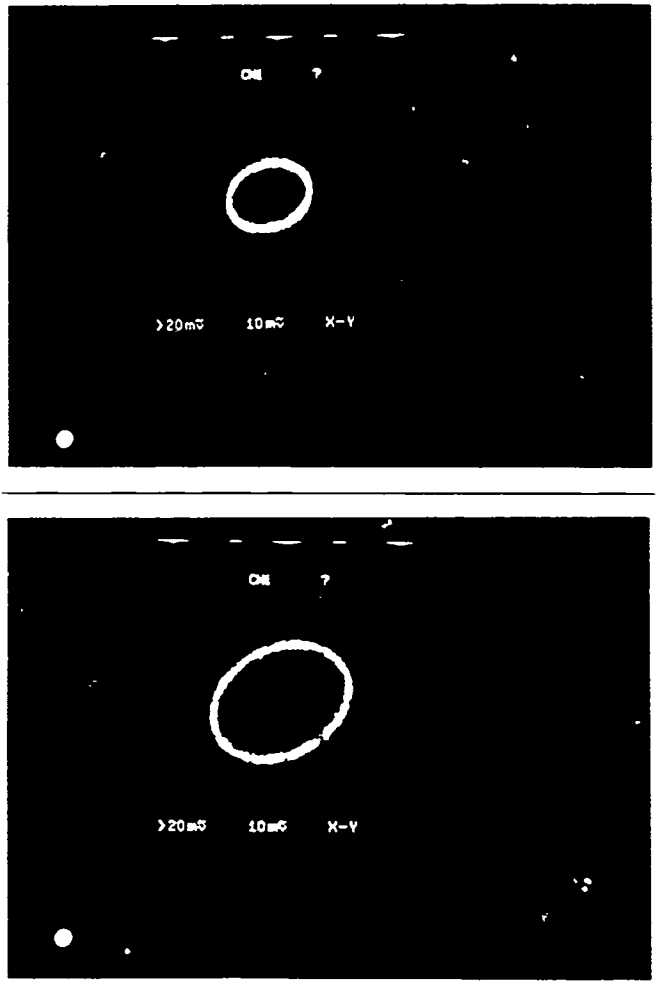

Figure 18. Photograph of Lissajous figures from detector outputs subjected to induced turbulence.

IV. CONCLUSIONS AND RECOMMENDATIONS

A. CONCLUSIONS

As stated in the introduction, the principle goal to this thesis project was to develop and to implement a proof-of-concept validation of a two-beam, division of wavefront laser interferometer that provides real time measurements of optical path differences caused by atmospheric turbulence. The photographs and results cited in Chapter III offer proof that this goal was achieved and that the underlying concepts are sound. However further development and testing is required before the system could be upgraded to a working field instrument for the collection of turbulence data over various geographic areas and atmospheric conditions.

For the laboratory prototype, the most difficult aspects were maintaining a stable signal and eliminating the ambient electrical signal/noise interference that adversely impacted both detector output signals to the receiver. The interference, of undetermined origin, proved a major obstacle in achieving correct, accurate signal processing in the receiver. Specifically, the interference made it difficult to match the gains of the two detector signals and created difficulty in effectively filtering the dithering signal at the receiver's passband filter. The lack of a stable signal created further difficulty in maintaining the threshold voltage required by receiver's Schmitt trigger. A upgraded production version of this system will incorporate higher precision optics and electronics and a more sophisticated means to isolate detector output signals so as to minimize the interference and stability problems experienced in this work.

B. RECOMMENDATIONS

The aforementioned problems of prototype stability and sustainability did not allow for a full range of testing over various distances and atmospheric conditions. Such tests and

data collection are recommended for future research. Such future work should incorporate a radio transmitted dithering signal between the transmitter and receiver assemblies instead of the coaxial cable connection used in this prototype design.

The prototype of this thesis operated in a relatively benign laboratory environment. As constructed the prototype optics would not readily maintain their alignment if subjected to constant repositioning and to exposure of the elements. Future work should therefore seek to develop a more precise, stable and weatherproof mechanism to house the optical arrangements of both the receiver and transmitter units. Such an optical mounting device would certainly ease the testing process and reduce the stability/robustness problems encountered in this work.

LIST OF REFERENCES

1. Lennox, Duncan ed., *Jane's 1990 Strategic Weapons Systems*, Jane's Information Group, 1990.

2. Collins, Graham P., "Making Stars to See Stars: DOD Adaptive Optics Work Declassified," *Physics Today*, pp. 17-21, February 1992.

3. Davis, D.S. and Walters, D.L., Memorandum to Phillips Laboratory,Subject: Stratospheric, Horizontal Path Optical Measurements, 31 January 1992.

4. Davis, D.S. and others, "Infrared Fourier Spectrometer for Airborne and Ground-based Astronomy," *Applied Optics*, v. 19, 1980.

5. Tyson, Robert K., *Principles of Adaptive Optics*, pp. 17-36, Academic Press, Inc., 1991.

6. Pedrotti, Frank L. and Pedrotti Leno S., *Introduction to Optics*, pp. 257-262, Prentice-Hall, Inc., 1987.

7. Horowitz, P. and Hill, W., *The Art of Electronics*, 2nd ed., Cambridge University Press, 1989.

INITIAL DISTRIBUTION LIST

1.	Defense Technical Information Center Cameron Station Alexandria, VA 22304-6145	2
2.	Library, Code 52 Naval Postgraduate School Monterey, CA 93943-5002	2
3.	Professor K.E. Woehler, Code PH/Wh Chairman, Department of Physics Naval Postgraduate School Monterey, CA 93943-5000	1
4.	Assoc. Professor D.S. Davis, Code PH/Dv Department of Physics Naval Postgraduate School Monterey, CA 93943-5002	3
5.	Assoc. Professor D.L. Walters, Code PH/We Department of Physics Naval Postgraduate School Monterey, CA 93943-5000	1
6.	Department of Physics Library, Code PH Naval Postgraduate School Monterey, CA 93943-5000	2
7.	LCDR. C.S. Barbour, USN 204 Sunrise Bluff Ln. Smithfield VA, 23430	2